NASA/CR-1999-209120/VOL4

# Acoustic Treatment Design Scaling Methods

*Volume 4: Numerical Simulation of the Nonlinear Acoustic Impedance of a Perforated Plate Single-Degree-of-Freedom Resonator Using a Time-Domain Finite Difference Method*

R. E. Kraft
*General Electric Aircraft Engines, Cincinnati, Ohio*

April 1999

# Abstract

Single-degree-of-freedom resonators consisting of honeycomb cells covered by perforated facesheets are widely used as acoustic noise suppression liners in aircraft engine ducts. The acoustic resistance and mass reactance of such liners is known to vary with the intensity of the sound incident upon the panel. Since the pressure drop across a perforated liner facesheet increases quadratically with the flow velocity through the facesheet, this is known as the nonlinear resistance effect. In the past, two different empirical frequency domain models have been used to predict the Sound Pressure Level effect of the incident wave on the perforated liner impedance, one that uses the incident particle velocity in isolated narrowbands, and one that models the particle velocity as the overall velocity. In the absence of grazing flow, neither frequency domain model is entirely accurate in predicting the nonlinear effect that is measured for typical perforated sheets. The time domain model is developed in an attempt to understand and improve the model for the effect of spectral shape and amplitude of multi-frequency incident sound pressure on the liner impedance. This is of particular concern with regard to frequency-scaling of acoustic treatment, since the possibility exists that the nonlinear resistance and mass reactance effects may be significant compared to the grazing flow effects at high frequencies. A computer code for the time-domain finite difference model is developed and predictions using the models are compared to current frequency-domain models.

# Table of Contents

# Numerical Simulation of the Nonlinear Acoustic Impedance of a Perforated Plate Single-Degree-of-Freedom Resonator Using a Time-Domain Finite Difference Method

## 1. General Theory

### 1.1. Introduction

#### 1.1.1. Background

Single-degree-of-freedom (SDOF) resonators consisting of thin-walled honeycomb tubular cells covered by a porous faceplate are the simplest form of acoustic lining in use as noise suppression treatment in aircraft engine ducts. Figure 1 shows the typical construction of an SDOF treatment panel, for which the significant parameters are the cavity depth, L, the faceplate thickness, t, the orifice hole diameter, d, and the faceplate open area ratio, or porosity, $\sigma$. The design of SDOF liners consists of determining the particular combination of parameters that provides the best suppression performance under the design constraints.
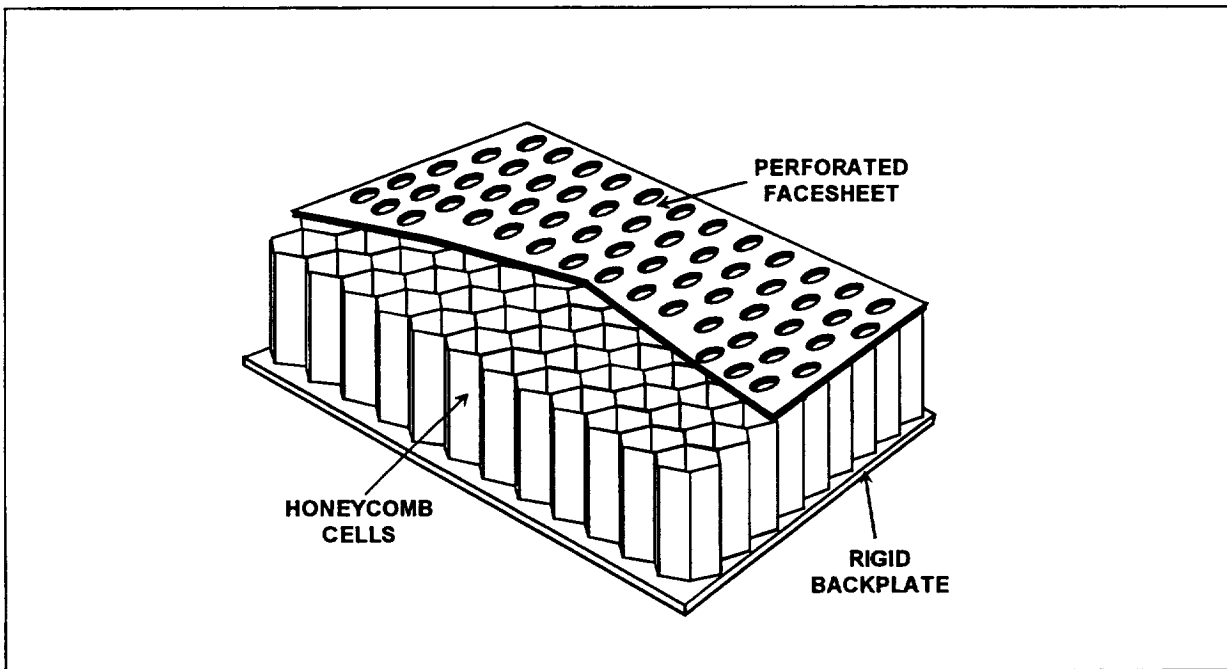


Figure 1.     Typical construction of SDOF treatment panel.

The design is complicated by the fact that SDOF liners covered by perforated orifice sheets behave nonlinearly, that is, their acoustic impedance is a function of the Sound Pressure Level (SPL) of the sound wave incident on the surface. This nonlinear behavior arises due to the resistance to flow through an orifice, which is such that the pressure drop across the orifice is a quadratic function of the DC flow velocity through the orifice:

1

$$\Delta p = A \cdot U + B \cdot U^2 \tag{1}$$

where A and B are constants that will be specified later and U is the through-flow velocity incident on the facesheet. The acoustic resistance of the resonator, which is the complex ratio of incident acoustic pressure to acoustic velocity at the surface of the liner, thus depends on the acoustic velocity, which in turn depends on the response of the liner, which is initially unknown. An iteration must be performed on the acoustic velocity to determine the acoustic impedance. Fortunately, this iteration generally converges quite rapidly.

The acoustic impedance of SDOF perforated plate resonators is usually predicted using frequency-domain models in closed form, with the exception of the velocity iteration[1]. It has been found that the impedance at a given frequency depends not only on the acoustic velocity in a narrowband frequency range surrounding the frequency, but also on contributions from acoustic velocities at other frequencies. Two empirical models currently exist to determine the acoustic velocity to be used at each frequency, and the two models are at opposite extremes. The first model uses the acoustic velocity in a narrowband around the frequency of calculation, so that the acoustic SPL applied is the pressure attributed to that narrowband range. The other model uses the square root of the overall sum of acoustic velocities for the entire pressure spectral range,

$$v_n = \sqrt{\sum_{i=1}^{N_{frq}} v_i^2} \tag{2}$$

where n is the index for the frequency of calculation and $N_{frq}$ is the total number of frequencies. The narrowband velocity assumption tends to underpredict the resistance, but the overall velocity assumption, which is the more accurate, still tends generally to obscure the finer variations in resistance due to pressure spectrum shape.

Although the frequency-domain models account for the resistance nonlinearity and are efficient to apply, they omit an important part of the physical process. The nonlinearity in damping causes the acoustic velocity at the faceplate to become non-sinusoidal, thus scattering energy into higher harmonics of frequency. This energy scattered from lower to higher frequencies will have an effect on the impedance at higher frequencies. To properly account for this energy scatter requires a time-domain model. This may be particularly important at very high frequencies for scale model treatment panels.

### 1.1.2. Objectives

The objective of this study is to develop a numerical time-domain model that simulates the nonlinear impedance effects of an SDOF resonator consisting of a perforated plate over a finite depth cavity. Since acoustic impedance is fundamentally a frequency-domain quantity, the model converts the acoustic pressure and velocity solution from the time domain to the frequency domain to predict the acoustic impedance over a range of frequencies, given an input SPL

spectrum. The purpose of this report is to document the analysis, provide a guide to use of the computer program, and make a limited preliminary model assessment by comparing time-domain predictions, frequency-domain predictions, and measured data.

The computer impedance prediction model in its current form must be considered to be a preliminary version. For increased utility, it will be possible to include more advanced models of the velocity or displacement dependence of the orifice end effects, the effects of grazing flow on the nonlinear impedance, and the time-dependent effects on the linear resistance term. The program will allow computer experiments with various assumptions regarding the physical parameters. In particular, it is hoped that the model will allow investigation of effects of frequency scaling, that is, behavior at low Reynolds's numbers and high frequencies.

### 1.1.3. Historical Background

Several researchers have considered the solution to the acoustic properties of a perforated plate from a numerical integration point of view. Rice[2] was one of the first to analyze the nonlinear behavior of a perforated sheet liner using a time-domain numerical integration approach. In his paper, Rice develops a nonlinear resistance model for the effect of multiple frequency excitation. The method also includes the effect of steady grazing flow and a high frequency, small displacement effect. Rice remarks on the difficulty of including an accurate model for the linear resistance term, which is frequency-dependent, and develops an approximate formulation, but notes that generally the contribution of the linear resistance term is small in the presence of grazing flow for conventional perforates. Rice models a finite depth cavity using a four-element lumped mass reactance and stiffness reactance model, which allows the cavity response to be approximated using transmission line theory rather than using an actual finite difference solution.

Cummings[3] developed a one-dimensional numerical time-domain model to simulate the nonlinear resistance of a perforated plate. Cummings' models allow several different termination conditions on the right side of the faceplate: an infinite tube ($\rho c$ termination); an infinite baffle termination; or a small volume Helmholtz resonator termination (maximum cavity dimension much less than a wavelength). These choices of geometry reduce the (nonlinear) integration to an integration in time only, eliminating the need for a spatial numerical integration in the spatial region to the right of the faceplate.

Cummings was interested primarily in determining the acoustic transmission loss through the perforated plate, as opposed to the impedance at the facesheet. He considers primarily transient pressure excitation (tone bursts and pulses). His numerical results show excellent agreement with experimental measurements made as part of the study. Cummings also includes an empirical model for time variation of the end effect.

Zorumski and Parrott[4], using a Fourier decomposition approach, derive a formula for the nonlinear effect of high amplitude, multiple-frequency pressure excitation on acoustic impedance of a perforate. The method is based on the DC flow resistance measured for the perforate and indicates that the impedance at any frequency is a function of the overall acoustic velocity

3

summed over all frequencies. Zorumski and Tester[5] and Rice[6] argue that the particle velocity at each frequency should be replaced by the total effective particle velocity summed over all frequencies.

Hersh and Rogers[7], Hersh and Walker[8], and Hersh[9] have developed a fluid mechanical model for nonlinear orifice behavior in which they assume the particle velocity approaches the orifice in a spherical manner. The analysis is limited to a calculation at the tuning frequency of a Helmholtz resonator, which is assumed to be known. The analysis is semi-empirical in that it requires measured data to determine two key parameters, an effective orifice radius and an effective orifice discharge coefficient. The solution for the nonlinear resistance is obtained numerically by integrating a second-order differential equation in the time domain. Other than the differences in the equations due to the initial orifice flow assumptions, the method of Hersh is quite similar to that of Cummings.

The development of the model in this report is based directly on the work of Rice and on the work of Cummings (which is, in turn, based on the preceding work of Cummings and Eversman[10]). The unique element of this effort is the incorporation of a central difference numerical integration scheme to account accurately for the effects of a resonator cavity of arbitrary depth.

### 1.1.4. Assumptions

The model is one-dimensional in space, so that only a plane wave is assumed to be incident upon and propagate within the cavity. The input acoustic pressure on the perforated plate surface is given. The acoustic resistance and mass reactance of the faceplate are assumed to be lumped in a thin sheet, where the sheet thickness and orifice hole diameter are much less than the shortest wavelength considered.

For this preliminary development, the mass reactance of the perforate orifices is assumed to be constant (i.e., the end effects are assumed not to be a function of velocity), and the orifice discharge coefficient is assumed to be constant in time. The end effects are incorporated through the input of an arbitrary equivalent orifice length. It is assumed that wave attenuation due to viscous effects for propagation inside the cavity can be neglected.

### 1.2. Description of Acoustic Model

### 1.2.1. Model Geometry

The acoustic model of the SDOF resonator, shown in Figure 2 , is that of a resonator cell mounted at the end of a long tube. The diameter of the tube is sufficiently small that only the plane wave is cut-on (propagates unattenuated) at the highest frequency of interest. The tube is assumed to be terminated with a piston source some arbitrary distance from the facesheet on the

left. A pressure wave traveling to the right with a known frequency and amplitude content impinges on the treatment surface.
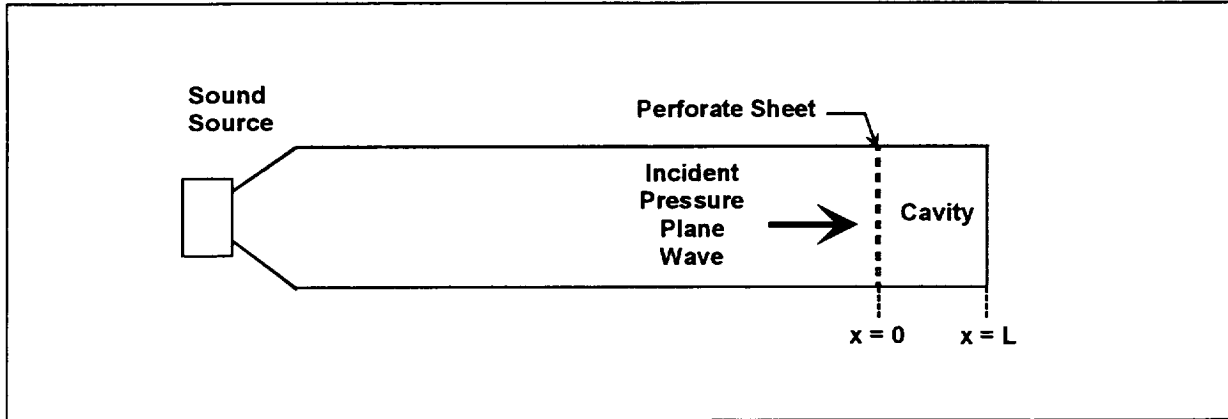


**Figure 2.    Acoustic model for SDOF resonator with normally-incident wave.**

The acoustic properties of the perforated plate are lumped at the plane of the faceplate, and a hardwall reflecting surface is located a known depth behind the faceplate. The input to the model is the acoustic pressure on the left side of the faceplate, which is combined with the lumped faceplate resistance and mass reactance to provide the left boundary condition for the cavity. The acoustic one-dimensional wave equation determines the propagation inside the cavity, and a hardwall, zero particle displacement condition is the right-hand boundary condition.

## 1.3.    Acoustic Wave Equation for Particle Displacement

The partial differential equation for the acoustic wave propagation is written in terms of acoustic particle displacement. The acoustic particle velocity, $\xi$, can be related to the "strain" of the medium as

$$\text{Strain} = \frac{\partial \xi}{\partial x} \tag{3}$$

where x is the spatial variable. The one-dimensional constitutive equation for the medium can be written as

$$p = -\Lambda \frac{\partial \xi}{\partial x} \tag{4}$$

where p is acoustic pressure and $\Lambda$ is the bulk modulus, which for air is

$$\Lambda = \rho c^2 \tag{5}$$

5

where $\rho$ is the density of the medium and c is the speed of sound. The acoustic particle velocity is given by

$$v = \frac{\partial \xi}{\partial t} \tag{6}$$

The wave equation for acoustic particle displacement inside the cavity is

$$\frac{\partial^2 \xi}{\partial x^2} = \frac{1}{c^2} \frac{\partial^2 \xi}{\partial t^2} \tag{7}$$

This will be expressed in central difference form below.

## 1.4.    Boundary Condition for Perforated Sheet and Cavity

At x = L the boundary condition for particle displacement is simply

$$\xi = 0 \tag{8}$$

which reflects the hardwall boundary requirement of zero particle displacement (and velocity).

The acoustic boundary condition at x = 0 is derived from the momentum balance equation and the fact that the acoustic velocity is continuous across the facesheet (i.e., acoustic velocity must be equal by continuity just to the left and to the right of the facesheet). The pressure applied to the fluid in the cavity just to the right of the facesheet will be the incident pressure at the left of the facesheet minus the pressure drop across the facesheet due to resistive and inertial effects. The pressure to the right of the facesheet must be balanced by the restoring force of the elastic medium in the cavity. This can be expressed as:

$$p(t) - M\frac{\partial^2 \xi}{\partial t^2} - D\frac{\partial \xi}{\partial t} = -\Lambda\frac{\partial \xi}{\partial x} \tag{9}$$

where M is the effective mass per unit area, and D is the effective damping per unit area. The particle displacement $\xi$ is the value averaged over the area of the facesheet.

The effective mass per unit area can be written as

$$M = \frac{\rho\ell}{\sigma C_d} \tag{10}$$

where $\ell$ is the effective orifice length (sheet thickness plus end effects), $\sigma$ is the open area ratio or porosity, defined as the area of the holes divided by the corresponding area of the facesheet, and

6

$C_d$ is the orifice discharge coefficient. The orifice discharge coefficient is defined as the area of the vena contracta of the flow from the orifice divided by the geometric area of the orifice. To begin, we will consider only the linear part of the facesheet resistance $R_L$, which can be taken as the DC flow coefficient A, from Equation (1), so we take

$$D = R_L \tag{11}$$

The damping force term will later be extended to include the effects of nonlinear terms.

## 1.5.    Time Scale Transformation and Numerical Stability

We now make a change to the time scale of the differential equation and boundary conditions. If we let

$$\tau = ct \tag{12}$$

then the wave equation from Equation (7) is transformed to

$$\frac{\partial^2 \xi}{\partial x^2} = \frac{\partial^2 \xi}{\partial \tau^2} \tag{13}$$

and the boundary condition, Equation (9) becomes

$$-\left[\frac{\rho \ell c^2}{\sigma C_D}\right]\frac{\partial^2 \xi}{\partial t^2} - R_L c \frac{\partial \xi}{\partial t} + p(t) + \Lambda \frac{\partial \xi}{\partial x} = 0 \tag{14}$$

We substitute for $\Lambda$ from Equation (5) and normalize by $\rho c^2$ to get the non-dimensionalized form of the boundary condition at x = 0:

$$-\left[\frac{\ell}{\sigma C_D}\right]\frac{\partial^2 \xi}{\partial t^2} - \frac{R_L}{\rho c}\frac{\partial \xi}{\partial t} + \frac{1}{\rho c^2}p(t) + \frac{\partial \xi}{\partial x} = 0 \tag{15}$$

This will be the form of the partial differential equation and boundary conditions to which the central difference formulation is applied for the numerical integration. We define a numerical integration step size in x as $\Delta x$ and a step size in t as $\Delta t$.

As described in numerous references on numerical integration of partial differential equations[11,12,13,14], the convergence and stability of the numerical integration is obtained when the ratio of $\Delta x$ to $\Delta \tau$ is less than or equal to 1.0, or, choosing the equality condition, then

$$\Delta x = \Delta \tau = c\Delta t \tag{16}$$

7

This is equivalent to integrating along a characteristic line of the acoustic wave propagation, and is the condition used in the central difference scheme for this analysis.

## 1.6. Calculation Scheme and Output

The numerical integration problem for the SDOF resonator is of the initial value type. The medium in the cavity is at rest at time zero, at which time a forcing function (the incident plane wave pressure) is applied to the outside surface of the perforated faceplate. An initial transient will occur in the cavity as the pressure wave propagates along the cavity and is reflected from the hard end. Eventually, a steady-state pressure field response will be achieved in the cavity (transient responses will be damped by the facesheet).

The numerical integration is modeled in space-time as shown in Figure 3, which illustrates the x-t computation point grid. The space points are denoted by the index i and the time points by the index j, such that the $i^{th}$ spatial position is given by

$$x_i = i\Delta x \qquad\qquad i = 0,1,2,\dots,N \qquad\qquad (17)$$

and the $j^{th}$ time value is given by

$$\tau_j = j\Delta\tau \qquad\qquad j = 0,1,2,\dots,\infty \qquad\qquad (18)$$

Note that there are N+1 space divisions in the cavity and that the hardwall is located at $x = L = N\Delta x$.

The general outline of the computational simulation of SDOF resonator impedance is shown in Figure 4. The incident pressure is applied at the outer surface of the perforated sheet by "ramping up" the pressure to its final amplitude over a given number of periods of the lowest frequency in the pressure signal. The computation is then given a number of longest periods plus several cavity traverse times as settling time for the transients.
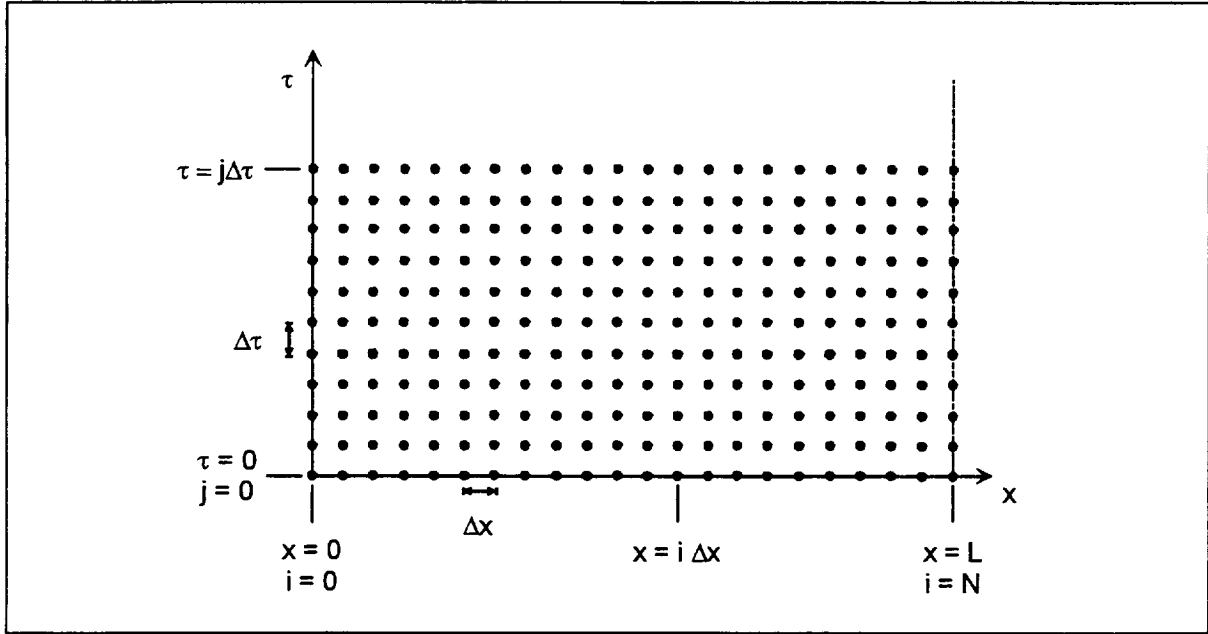
**Figure 3**    Computational grid for perforated plate/resonator cavity impedance time-domain numerical integration model.
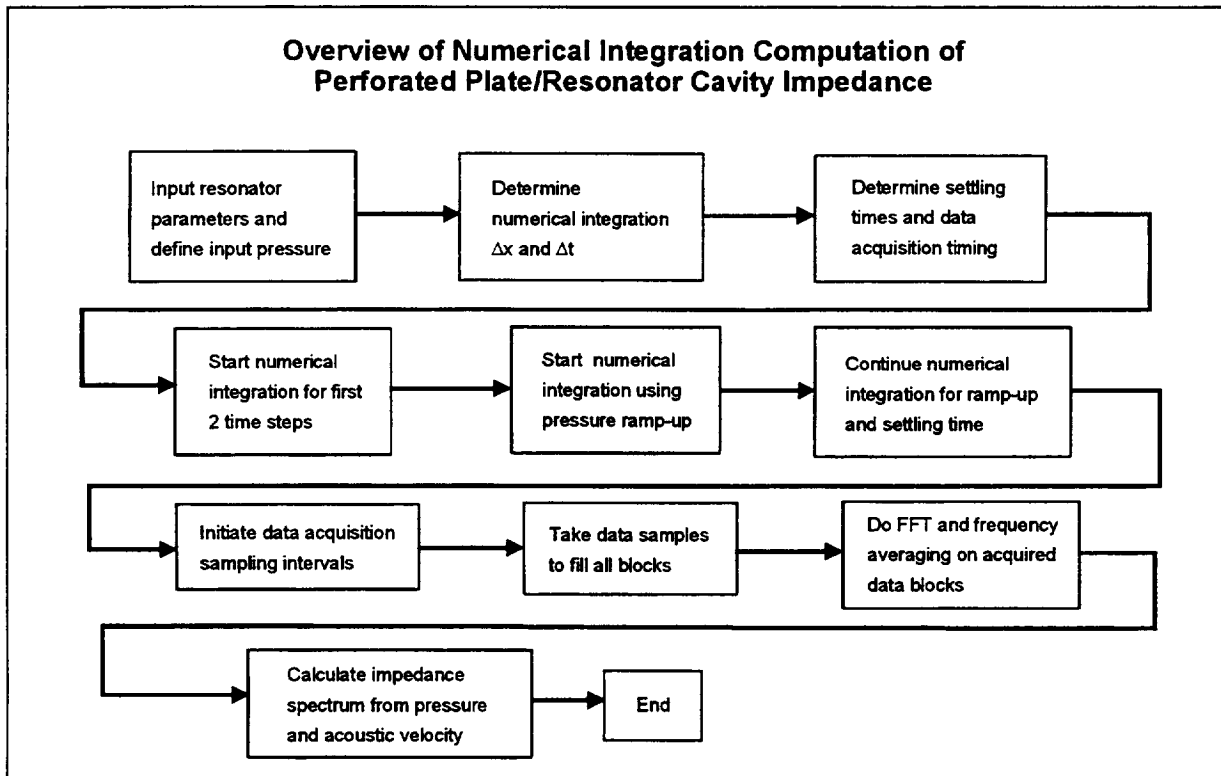


**Figure 4.**    Flowchart for numerical integration computation of perforated plate/resonator cavity impedance.

After the solution has achieved steady state, the first data acquisition sequence is initiated, and the time, pressure and acoustic particle displacement are stored in a block as if they were being measured as a digitized time series. The acquisition of data blocks continues until the number of blocks specified for frequency averaging has been acquired. The numerical integration time step may be much finer than the data acquisition time step, so that there may be many more points calculated than acquired for the Fourier analysis.

Fast Fourier Transforms are performed on the time history data blocks, giving frequency-averaged acoustic pressure and particle displacement spectra. The acoustic velocity is computed as $i\omega$ times the acoustic particle displacement, where $\omega = 2\pi f$, and the impedance spectrum is found by dividing acoustic pressure by acoustic velocity in each frequency band.

Output files are obtained for the time histories of the input pressure and resulting particle displacement and velocity, as well as for the pressure, acoustic velocity, and impedance spectra. The output files can be used as input to standard plotting routines (or spreadsheets) to obtain graphical output.

## 2. Finite Difference Equation Formulation - Linear Form

### 2.1. Central Difference Formulation for the Partial Differential Equation

Using the index i to denote x grid points and the index j to denote $\tau$ grid points, the acoustic particle displacement at position i and time j can be written as $\xi_{i,j}$. The finite difference forms for the first and second derivatives are given by

$$\frac{\partial \xi}{\partial \tau} = \frac{\xi_{i,j+1} - \xi_{i,j-1}}{2\Delta\tau} \qquad (19)$$

$$\frac{\partial \xi}{\partial x} = \frac{\xi_{i+1,j} - \xi_{i-1,j}}{2\Delta x} \qquad (20)$$

$$\frac{\partial^2 \xi}{\partial \tau^2} = \frac{\xi_{i,j+1} - 2\xi_{i,j} + \xi_{i,j-1}}{(\Delta\tau)^2} \qquad (21)$$

$$\frac{\partial^2 \xi}{\partial x^2} = \frac{\xi_{i+1,j} - 2\xi_{i,j} + \xi_{i-1,j}}{(\Delta x)^2} \qquad (22)$$

The central-difference formulation for the partial differential equation (13) can be written

$$\frac{\xi_{i+1,j} - 2\xi_{i,j} + \xi_{i-1,j}}{(\Delta x)^2} = \frac{\xi_{i,j+1} - 2\xi_{i,j} + \xi_{i,j-1}}{(\Delta\tau)^2} \qquad (23)$$

Using the stability relation from Equation (16), this can be simplified to

$$\xi_{i,j+1} = \xi_{i-1,j} + \xi_{i+1,j} - \xi_{i,j-1} \qquad (24)$$

Figure 5 shows graphically how the particle displacement at time j+1 is related to the displacement at prior times and locations.

11
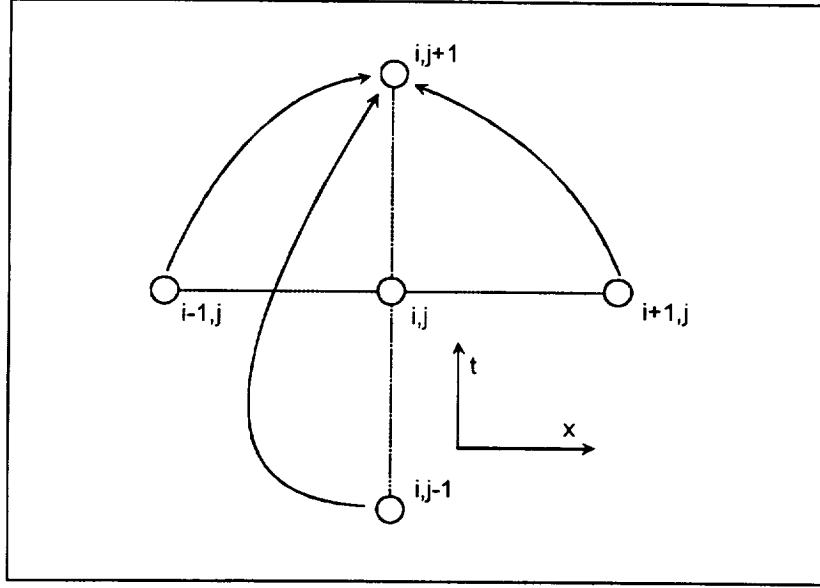
**Figure 5.** **Particle displacement time-step prior influence graph.**

## 2.2. Central Difference Formulation for the Boundary Conditions

The finite difference form for the boundary condition at $x = L$, $i = N$ is simply

$$\xi_{N,j} = 0 \tag{25}$$

for all j-values, since the acoustic particle displacement is zero at the hard wall.

The finite difference form of the boundary condition at $x = 0$, Equation (15), is

$$\left(\frac{m}{h^2} + \frac{R}{2h}\right)\xi_{0,j+1} - \frac{2m}{h^2}\xi_{0,j} + \left(\frac{m}{h^2} - \frac{R}{2h}\right)\xi_{0,j-1} + \frac{1}{\rho c^2}p_j + \frac{1}{2h}\left(\xi_{1,j} - \xi_{-1,j}\right) = 0 \tag{26}$$

where we define

$$h = \Delta\tau \tag{27}$$

$$m = -\frac{\ell}{\sigma C_D} \tag{28}$$

and

$$R = -\frac{R_L}{\rho c} \tag{29}$$

12

Equation (26) can be further simplified to the form

$$C_1\xi_{0,j+1} + C_2\xi_{0,j-1} - C_3\xi_{0,j} + C_4\left(\xi_{1,j} - \xi_{-1,j}\right) + C_6 p_j = 0 \qquad (30)$$

where

$$C_1 = \frac{m}{h^2} + \frac{R}{2h} \qquad (31)$$

$$C_2 = \frac{m}{h^2} - \frac{R}{2h} \qquad (32)$$

$$C_3 = \frac{2m}{h^2} \qquad (33)$$

$$C_4 = \frac{1}{2h} \qquad (34)$$

and

$$C_6 = \frac{1}{\rho c^2} \qquad (35)$$

(The coefficient $C_5$ has been reserved for later use.) Note that the boundary condition equation requires the definition of a fictitious particle displacement at the i = -1 grid point in x, one step to the left of the boundary condition surface.


## 2.3. Initial Conditions

The initial conditions on particle displacement are defined along the first horizontal row of finite difference grid points, defined by the line j = 0 (for $\tau$ = 0). Since the medium starts at rest, we also require that the acoustic velocity is zero along this line. These conditions are given in finite difference form as

$$\xi_{i,0} = 0 \qquad (36)$$

and

$$\xi_{i,1} - \xi_{i,-1} = 0 \qquad (37)$$

13

for all i values. Note that the velocity initial condition requires the specification of the particle displacement at the j = -1 time step.

## 2.4. Step-Up and Step-Across Algorithms

To visualize how the numerical integration will proceed, we define two integration algorithms, the Step-Across algorithm and the Step-Up algorithm, "across" referring to the space dimension and "up" referring to time.

Consider $\xi$ for any succeeding time step at x = 0 (i = 0). Equations (24) and (30) can be combined to give

$$\xi_{0,j+1} = -D_1 p_j - D_2 \xi_{0,j-1} + D_3 \xi_{0,j} - D_4 \xi_{1,j} \tag{38}$$

where

$$D_1 = \frac{C_6}{C_1 - C_4} \tag{39}$$

$$D_2 = \frac{C_2 - C_4}{C_1 - C_4} \tag{40}$$

$$D_3 = \frac{C_3}{C_1 - C_4} \tag{41}$$

and

$$D_4 = \frac{2C_4}{C_1 - C_4} \tag{42}$$

This is the Step-Up algorithm, which gives the next time increment from prior time values at the faceplate. The Step-Up algorithm, since it is defined at x = 0, incorporates the perforated plate boundary condition into the solution.

With the next highest time value (j+1) given at the left edge, we can then step across to fill in the row j+1 (i = 1 to N) using Equation (24), which becomes the Step-Across algorithm. Once the first two rows are determined using the initial conditions, the rest of the solution can be found for all times. The Step-Across algorithm incorporates the resonator cavity response into the solution.

When the Step-Across algorithm is used to fill in all rows for j = 1 and higher, the zero acoustic displacement boundary condition at x = L (i = N) must be enforced.

14

## 2.5. Starting the Numerical Integration

The $\xi$ values for the first row are already given in Equation (36). To obtain the second row, we use Equation (38) at $j = 0$ and the initial condition on acoustic velocity in Equation (37) at $i = 0$ to obtain the particle displacement at $i = 0$ and $j = 1$,

$$\xi_{0,1} = \frac{D_4}{1 + D_2} p_0 \qquad (43)$$

The Step-Across algorithm can be used to fill in the rest of row two. Making the substitutions, it can be shown that $\xi_{i,1}$ is zero for all $i$. This is not surprising, for the acoustic perturbation which has just initiated due to turning on the incident pressure at the surface has had no time to propagate into the cavity.

# 3. Incorporation of the Nonlinearity in the Boundary Condition

## 3.1. Boundary Condition Equation

We now add a nonlinear resistance term to the perforated plate pressure-balance boundary condition, so that it takes the form

$$\frac{1}{\rho c^2}p - \frac{R_L}{\rho c}\frac{\partial \xi}{\partial \tau} - \frac{R_{NL}}{\rho}\frac{\partial \xi}{\partial \tau}\left|\frac{\partial \xi}{\partial \tau}\right| - \frac{\ell}{\sigma C_D}\frac{\partial^2 \xi}{\partial \tau^2} + \frac{\partial \xi}{\partial x} = 0 \qquad (44)$$

where $R_{NL}$ is the nonlinear resistance coefficient which can be identified with the coefficient B in the DC flow resistance given in Equation (1). The absolute value of the velocity must be taken to assure that positive damping occurs on both sides of the acoustic velocity cycle.

It is useful to review the physical interpretation of each of the terms in the perforated plate boundary condition equation. The first term is due to the applied acoustic pressure, p, on the perforate outside surface. The second term is the linear contribution to the damping force, proportional to the particle velocity. The third term is the nonlinear contribution to the damping force, proportional to the square of the acoustic velocity. Together, the two damping terms are equivalent to those that would be obtained from a DC flow resistance measurement, making the identification of the rms value of the acoustic velocity with the magnitude of the DC flow velocity. The fourth term is the inertance contribution of the mass reactance, dependent upon an equivalent orifice length, $\ell$. The last term is the restoring force due to the compression of the elastic medium in the cavity at x = 0.

## 3.2. Finite Difference Formulation

Equation (44) can be expressed in finite difference form as

$$\xi_{0,j+1} = -D_1 p_j - D_2 \xi_{0,j-1} + D_3 \xi_{0,j} - D_4 \xi_{1,j} + D_5\left(\xi_{0,j+1} - \xi_{0,j-1}\right)\left|\xi_{0,j+1} - \xi_{0,j-1}\right| \qquad (45)$$

where $D_1$ through $D_4$ have the same definitions as given previously,

$$D_5 = \frac{C_5}{C_1 - C_4} \qquad (46)$$

and where

$$C_5 = \frac{R_{NL}}{4\rho h^2} \qquad (47)$$

16

$C_1$ through $C_4$ have the same definitions as before. Equation (45) cannot be solved explicitly for $\xi_{0,j+1}$, and must be solved by an iterative technique.

## 3.3. Nonlinear Velocity Iteration Algorithm

The particle displacement at time $j+1$ is extracted from the nonlinear equation (45) using a Newton-Raphson iteration technique. We write the equation in the form

$$f(\xi_P) = D_5(\xi_P - \xi_M)|\xi_P - \xi_M| + T_1 - \xi_P \tag{48}$$

where

$$\xi_P = \xi_{0,j+1} \tag{49}$$

$$\xi_M = \xi_{0,j-1} \tag{50}$$

and

$$T_1 = -D_1 p_j - D_2 \xi_{0,j-1} + D_3 \xi_{0,j} - D_4 \xi_{1,j} \tag{51}$$

The quantities $\xi_M$ and $T_1$ are constant over the iteration.

The Newton-Raphson iteration is written in the form

$$\xi_P(n+1) = \xi_p(n) - \frac{f(\xi_p(n))}{f'(\xi_p(n))} \tag{52}$$

where n is the iteration number and where the prime denotes the derivative with respect to $\xi_P$. It can be shown that the derivative in the denominator takes on the same value for either $\xi_P > \xi_M$ or $\xi_P < \xi_M$, and that it is given in finite difference form by

$$f'(\xi_P) = 2.0 \cdot D_5 |\xi_P - \xi_M| - 1.0 \tag{53}$$

In most cases attempted so far, the iteration converges quite rapidly, although further work is needed to assure that this algorithm is working properly.

17

# 4. Numerical Integration Computer Program Operation

## 4.1. Computer Program

The computer program ZORF4 has been written to accomplish the numerical integration and time-series Fourier analysis leading to a prediction of the cavity resonator impedance. ZORF4 is written in FORTRAN for use on the IBM-PC. This FORTRAN version could be easily adapted for use on other computers.

Proper use of the program requires some insight to the methods by which the calculations are accomplished and how some of the input variables are interpreted and established. This section documents the use of the computer program.

## 4.2. Program Limitations

The dimensions of arrays in the computer program were sized based on estimates of the largest number of grid points in the x-direction that might be encountered for a reasonable problem. The acoustic particle displacement values (real, double precision) must be stored for only three rows of time values simultaneously. The values are written to a file on disk for each row as it is calculated. The maximum number of grid points in the x-direction is set at 5000 using the following reasoning:

1. Assume the maximum frequency encountered will be 40,000 Hz.
2. The speed of sound is nominally 34,000 cm/sec (room temperature value).
3. This gives a wavelength, $\lambda$, of about 0.85 cm at 40 KHz.
4. Assume the resonator cavity depths will be at most 10 of these shortest wavelengths (8.5 cm, about 3.3 in.)
5. The minimum desired grid spacing will use at most 500 points per wavelength.
6. Multiplying 10 wavelengths by 500 points per wavelength gives 5000 grid points, maximum.

The grid points are assumed to be equally spaced. Storage is not a problem for an IBM PC, so that the maximum array dimensions could be increased, if desired.

For the FFT spectral analysis, the maximum time sequence block size is 1024 points, and the value chosen must be a power of 2. The time interval FFT data sampling is chosen to be an integral number of numerical integration time steps, say $N_{samp}$, so that every nth data point is stored as the time history for spectral analysis. Up to 16 frequency averages are allowed.

## 4.3. Time Constants

### 4.3.1. Numerical Integration Time Step

The numerical integration time step is related to the numerical integration stability condition given in Equation (16). The integration distance step size will be some small fraction of a wavelength required to achieve convergence. Experience in running the program indicated that up to several hundred points per wavelength were required to achieve acceptable convergence. Denote the value of points per wavelength at the shortest wavelength (highest frequency), which is input to the program, as $N_{ppl}$. Then the distance step size is given by

$$\Delta x = \frac{c}{8 N_{ppl} F_{ph}} \qquad (54)$$

where $F_{ph}$ is the highest frequency component in the pressure input signal and c is the speed of sound. The multiplier 8 in the denominator is chosen because the highest frequency in the data analysis (the Nyquist frequency) is set to 8 times the highest frequency in the input signal.

The numerical integration time step, in normalized form $\Delta\tau$, is equal to $\Delta x$, by the stability criterion. The actual numerical integration time step will be $\Delta\tau$ divided by the speed of sound, or

$$\Delta t = \frac{1}{8 N_{ppl} F_{ph}} \qquad (55)$$

If the minimum $\Delta x$ is the shortest wavelength divided by 500, then the minimum numerical integration time step (in real time units) will be

$$\Delta t_{min} \cong \frac{\Delta x_{min}}{c} = \frac{\lambda_{min}}{500c} = \frac{0.85}{500*34,000} = 5 \times 10^{-8} \quad \text{seconds} \qquad (56)$$

where the minimum wavelength $\lambda_{min}$ of 0.85 cm. is based on the assumption of a highest frequency of interest of 40,000 Hz. and a minimum speed of sound of 34,000 cm/sec.

### 4.3.2. Transient Decay Time

Before initiating data acquisition of the acoustic displacement time history for spectral analysis, it is necessary to be assured that the solution has achieved steady state and any transients caused by "switching on" the applied pressure at time zero have decayed sufficiently to have negligible effect. The procedure used to set the elapsed time before initiating the first data acquisition is described in this section.

If we assume a maximum cavity depth of interest of 5 cm., then the longest time required for a plane wavefront to traverse the cavity in both directions will be

19

$$T_{cav\,max} = \frac{L}{c} = \frac{5\,cm}{34000\,cm/sec} \cong 3.0E-4 \quad sec \tag{57}$$

If we assume that the lowest frequency of interest is 100 Hz., then the maximum wave period will be

$$T_{per\,max} = 0.01 \quad sec \tag{58}$$

These quantities can be used to estimate a required solution "settling time" during which transients caused by switching on the applied pressure are allowed to decay. We are assuming that the damping inherent in the facesheet will always be sufficient to eventually eliminate the transient from the solution.

The acoustic pressure applied to the faceplate is obtained by summing a Fourier series of frequency components, and this pressure may not be zero at time zero. This finite jump in pressure at time zero will introduce a transient into the solution. To guarantee that the pressure starts from zero and builds slowly, a linear ramp function that extends over the first three longest periods (that is, the period of the lowest frequency component of the applied pressure), increasing from zero to one, is multiplied into the applied pressure.

Then a settling time equal to at least three more longest periods is added, with an option of adding as many additional longest periods as desired. Finally, a time period equal to the time required for the wave to traverse the cavity (one-way) four times is added. The only means of determining whether, in fact, the transient has decayed acceptably is to repeat the case with an increased length of delay interval and compare the results with the initial run.

## 4.4. Spectral Analysis

### 4.4.1. Data Sampling

When the process reaches a steady state, the data acquisition can be initiated. Time histories are acquired for the particle displacement and the applied pressure. Data is acquired in *blocks* in the same manner as it would be acquired by the analog-to-digital board of a digital spectral analyzer. FFT's are applied to each of the data blocks and the results are then frequency-averaged.

The pressure input frequencies are chosen such that they can be matched exactly by the data analysis output frequencies. This allows the use of a rectangular window, eliminating the need for more exotic windowing.[15] Some forethought is required for the initial choice of pressure frequencies, for they must align with the frequency bins of the FFT of the solution based on a data acquisition sample size that is a power of 2.

The numerical integration time step is much finer than the time step required for data sampling. The Nyquist frequency for the data analysis is set at 8 times the highest frequency in the pressure input signal. The sampling time interval $\Delta\tau$ commensurate with achieving this Nyquist frequency is given by

$$\Delta\tau_{samp} = \frac{c}{16F_{ph}} \tag{59}$$

The number of numerical integration time intervals per data sampling time interval is then given by

$$N_{samp} = \frac{\Delta\tau_{samp}}{\Delta\tau} = \frac{N_{ppl}}{2} \tag{60}$$

By choosing $N_{ppl}$ to be a multiple of 2, we guarantee that there will always be an integral number of time intervals between data sampling points. This is a convenience that makes it unnecessary to store the results of the numerical integration between data sampling points as long as the points are counted. Storing each integration point would be required if it were necessary to interpolate the results to the required data sampling time.

The block size of the data acquisition, $N_{blk}$, is provided as input. This must be an integer power of 2 for the convenience of the FFT. The data block record length is, then, in real time units,

$$T_{rec} = \frac{N_{blk}}{16F_{ph}} \tag{61}$$

and the frequency resolution of the resulting spectra is

$$\Delta f = \frac{16F_{ph}}{N_{blk}} \tag{62}$$

The maximum block size is $N_{blk} = 1024$, which give a finest frequency resolution of 1/64 of $F_{ph}$. Recall that the pressure input frequencies must be input at exactly these frequencies.

Some combinations of parameters $\Delta f$, $F_{ph}$, and $N_{blk}$ must be chosen at the start to assure the data analysis frequencies and pressure frequencies match (there may be more data analysis frequencies than pressure frequencies, but the pressure frequencies must align with data analysis frequencies). If pressure data is from a measured FFT spectrum, the values may have to be combined in different bandwidth frequency bins to fit the data requirements of ZORF4. The choice of these parameters may have to be guessed iteratively, and an artificial $F_{ph}$ with very low pressure values may have to be created to obtain the desired results.

21

## 4.4.2. Computation of Acoustic Pressure, Velocity, and Impedance

The acoustic pressure is needed at the surface of the perforated plate. The pressure is given as input to the problem, in terms of its frequency spectral components. To obtain the time history of the pressure at any arbitrary time, t, it is necessary to expand the Fourier components of the frequency,

$$p(t) = \sum_{n=1}^{NFP} PF_n e^{i\omega_n t} \tag{63}$$

where $PF_n$ is the $n^{th}$ complex spectral frequency component, $\omega_n$ is the $n^{th}$ circular frequency, and NFP is the number of frequencies with coefficients not equal to zero.

The pressure on the faceplate due to a normally-incident pressure wave is assumed to be known. Usually, only the acoustic pressure of the incident wave would be known, but the actual excitation pressure is that due to the combined incident and reflected waves at the surface. The reflected wave component, however, depends on the impedance of the surface, which is not known a priori.

If $P_{fwd}$ is the amplitude of the incident (forward-traveling) pressure wave for the $\omega$ component in the frequency domain, impinging on the facesheet from the left (outside the cavity), then the known forward-traveling part of the pressure wave is

$$p_{fwd}(x) = P_{fwd} e^{i(kx-\omega t)} \tag{64}$$

Using the impedance-matching boundary condition at the faceplate surface (x = 0), it can be shown that the resultant overall acoustic pressure at the faceplate outside surface is given by

$$p(0) = \frac{2P_{fwd}}{1+\alpha} \tag{65}$$

where

$$\alpha = \frac{\rho c}{Z} \tag{66}$$

is the normalized acoustic admittance of the surface. Note the expected pressure-doubling when the impedance is infinite (hardwall surface).

The SPL at the surface, then, must be determined from the rms magnitude of this resultant pressure,

22

$$|p(0)|_{rms} = \frac{2|P_{fwd}|_{rms}}{\sqrt{1 + Re(\alpha) + |\alpha|^2}} \qquad (67)$$

The input to ZORF4 is the complex resultant pressure p(0).

To obtain the incident pressure wave component that will provide a desired surface SPL, one must work backwards iteratively through the above equations, since the impedance may change as a function of pressure amplitude. Given only the incident pressure wave component, one would have to solve iteratively to determine the impedance, since it is a function of the resultant pressure, which in turn depends on the impedance.

The frequencies must be chosen to align with the frequency bins of the FFT data processing, and thus should be some integer multiple of $\Delta f$ as given in Equation (62). Note that it is not necessary to include a pressure spectral coefficient for each frequency between 0.0 and the highest frequency. The input could consist of only several widely spaced tones. The sum is over only those pressure coefficients with finite values, which saves some computation time.

The input pressure coefficients $PF_n$ should be in physical pressure units of dynes/cm$^2$ peak amplitude. The SPL is then computed from

$$SPL = 20\log\left(\frac{p}{\sqrt{2}(0.0002)}\right) \qquad (68)$$

where p is either the pressure in a spectral frequency bin or some combination of adjacent pressures.

The spectral components of the acoustic pressure are given, but the spectral components of the acoustic velocity must be obtained from an FFT of the acoustic displacement time history solution at the faceplate. If $X_n$ represents the n$^{th}$ spectral component of acoustic displacement at circular frequency $\omega_n$, then the n$^{th}$ component of acoustic velocity is given by

$$V_n e^{-i\omega_n t} = \dot{\xi}_n = -i\omega_n X_n e^{-i\omega_n t} \qquad (69)$$

or

$$V_n = -i\omega_n X_n = -i2\pi f_n X_n \qquad (70)$$

Given the pressure and velocity components at each frequency, the acoustic impedance normalized by $\rho c$ is simply

$$\frac{Z_n}{\rho c} = \frac{PF_n}{\rho c V_n} \qquad (71)$$

23

The real part of this is the acoustic resistance and the imaginary part is the acoustic reactance, both normalized by ρc.


## 4.5.    ZORF4 Program NAMELIST Input Guide

The computer program ZORF4 that implements the above analysis is written in FORTRAN code and runs on an IBM-PC compatible computer.  Input to the program is through a NAMELIST data file, as follows:

## ZORF4 NAMELIST INPUT GUIDE

*Time in sec, Displacements in cm., Pressure in dynes/cm^2, Velocity in cm/sec*
*DP implies a double precision variable*

&ZDAT

HEAD ='Case Title'    *Filenames up to 30 characters*

DFOUT='path/filename'  *Case data output file*

DFTHDAT='path/filename'  Time history of acquired data:

     *Formatted as Block# Sample# Time Pressure Displacement(0)*

DFTRNST='path/filename'  Transient time history up to start of D/A:

     *Formatted as TimePnt# Time Pressure Displacment(0)*

DFSPECT='path/filename'  Spectral data:

     *Formatted as Freq Prms SPL Vrms Zrcn*

RLIN=  Linear resistance (DC flow A-value) cgs Rayls (DP)

RNL=  Nonlinear resistance (DC flow B-value) cgs Rayls/(cm/sec)  (DP)

SIGMA=  Faceplate porosity (open area ratio) (DP)

DCAV=  Cavity depth, cm.  (DP)

RHO=  Air density, g/cm^3  (DP)

CS=  Speed of sound, cm/sec (DP)

EFFLGTH=  Effective orifice length, cm   (DP)

CD=  Orifice discharge coefficient  (DP)

CFNL=  Nonlinear term coefficient, set to 1.D0 or 0.D0

NFP=  Number of input frequencies

PF(1)=  Complex DP array of pressures at each frequency (peak amplitude, dynes/cm^2)

FRQP(1)=  DP array of frequencies for pressure input

NBLKSZ=  Data acquisition block size (power of 2, up to 1024)

NTDO=  Number of extra cycles for transient dieout, based on period of lowest frequency

NDSAMP=  Number of averages for frequency averaging, up to 16

/

25

The input data file should be given the name ZORF4IN.NML, and it should reside in the same directory as the ZORF4.EXE file. Be sure to back up prior NAMELIST data files that are to be saved with a different name. The output files are written to the directory and filename specified in the NAMELIST input.


## 4.6. Sample Case

A sample case was chosen to illustrate the use of the ZORF4 program. The case includes multiple frequency pressure input, with an applied pressure of 130 dB SPL in ten adjacent 125 Hz. bin width frequency bands from 875 Hz. to 2000 Hz. This case will be used later to compare the time domain numerical integration impedance model with the frequency domain model.

The basic input parameters for SDOF resonator are defined as follows:

Faceplate porosity = 5.0%
Faceplate thickness = 0.032 inches = 0.081 cm
Faceplate hole diameter = 0.132 inches = 0.132 cm
Cavity depth = 1.0 inches = 2.54 cm

Other constants are:

Air density = 0.001206 g/cm$^3$
Speed of sound = 34,394 cm/sec
Orifice discharge coefficient = 0.76
Absolute viscosity = 1.7894E-4 g/(cm-s)

These are characteristic of air at about 70 degF.

Additional inputs are the effective orifice length, the linear resistance, and the nonlinear resistance. These parameters, derived using equations given in the following section, are:

Effective orifice length = 0.176 cm
Linear resistance = 0.5020 cgs Rayls
Nonlinear resistance coefficient = 0.2088 cgs Rayls/(cm/sec)

The following is an input sheet for the ZORF4 run:

```
&ZDAT
HEAD='SAMPLE CASE #1'
DFOUT='SC1.OUT'
DFTHDAT='ZSC1.DAT'
DFTRNST='TSC1.DAT'
DFSPECT='SSC1.DAT'
RLIN=0.502D0
RNL=0.2088D0
```

```
SIGMA=.05D0
DCAV=2.54D0
RHO=.001206D0
CS=34394.D0
EFFLGTH=0.176D0
CD=.76D0
CFNL=1.0D0
NFP=10
PF(1)=(894.43D0,0.D0),(894.43D0,0.D0),(894.43D0,0.D0),(894.43D0,0.D0)
PF(5)=(894.43D0,0.D0),(894.43D0,0.D0),(894.43D0,0.D0),(894.43D0,0.D0)
PF(9)=(894.43D0,0.D0),(894.43D0,0.D0)
FRQP(1)=875.,1000.,1125.,1250.,1375.
FRQP(6)=1500.,1625.,1750.,1875.,2000.
NBLKSZ=256
NTDO=5
NDSAMP=3
/
```

The following is the main output run for this case, which was written into file SC1.OUT:

```
        PROGRAM ZORF4
   TIME DOMAIN CENTRAL DIFFERENCE MODEL FOR IMPEDANCE OF
   NONLINEAR SDOF RESONATOR COVERED BY PERFORATED PLATE

   TITLE: SAMPLE CASE #1

   RLIN =         .502000 cgs rayls
   RNL =          .208800 cgs rayls/(cm/sec)
   SIGMA =        .050000
   CAVITY DEPTH =      2.540000 cm
   EFFECTIVE CAVITY DEPTH =      2.536557 cm
   RHO =          .001206 g/cm^3
   CS =    34394.000000 cm/sec
   RHO*C =        41.479164 cgs Rayls
   EFFECTIVE ORIFICE LENGTH =       .176000 cm
    Cd =          .760000
   # OF PRESSURE FREQUENCIES =      10
   DATA ANALYSIS BLOCK SIZE =    256
   # DATA SAMPLE BLOCKS TAKEN =       3
   # INTEGRATION PNTS PER SHORTEST WAVELENGTH =     200
   # EXTRA CYCLES SETTLING TIME (NDTO) =     5
   # TIME STEPS TO D/A START = 30202

        OUTPUT DATA FILES:

   INPUT DATA AND PARAMETERS - SC1.OUT
   PRESS & VELOC TIME HIST - ZSC1.DAT
   INITIAL TRANSIENT TIME HIST - TSC1.DAT
   OUTPUT F,P,V,ZRC SPECTRA - SSC1.DAT


      J       FREQ         CMPLX PRESSURE COEFF        SPL

      1      875.00     8.944300E+02  0.000000E+00    130.00
      2     1000.00     8.944300E+02  0.000000E+00    130.00
      3     1125.00     8.944300E+02  0.000000E+00    130.00
      4     1250.00     8.944300E+02  0.000000E+00    130.00
      5     1375.00     8.944300E+02  0.000000E+00    130.00
      6     1500.00     8.944300E+02  0.000000E+00    130.00
```

27

```
   7    1625.00    8.944300E+02    0.000000E+00    130.00
   8    1750.00    8.944300E+02    0.000000E+00    130.00
   9    1875.00    8.944300E+02    0.000000E+00    130.00
  10    2000.00    8.944300E+02    0.000000E+00    130.00
```

```
LOWEST PRESSURE FREQ =      875.00 Hz
HIGHEST PRESSURE FREQ =    2000.00 Hz
UPPER ANALYSIS FREQUENCY =    16000.00 Hz
DATA ACQUISITION DELTA T =    3.1250D-05 sec
TIME STEP =   3.12500E-07 sec
HH or DELTA TAU =   1.07481E-02 cm

NONLINEAR TERM COEFF =        1.0000
CF1 =    -3.0471D+04
CF2 =    -3.0470D+04
CF3 =    -6.0941D+04
CF4 =     4.6520D+01
CF5 =     3.7468D+05
CF1 - CF4 =   -3.0517D+04
D1 =   -2.2969D-11
D2 =    9.9996D-01
D3 =    1.9969D+00
D4 =   -3.0487D-03
D5 =   -1.2278D+01
LONGEST CYCLE TIME =     1.1429D-03 sec
SETTLING TIME =    9.1429D-03 sec
CAVITY BOUNCE TIME =    7.3850D-05 sec
TIME TO START OF D/A =    9.4381D-03 sec
```

```
SAMPLE CASE #1

     FRQ        PRMS        SPL         VRMS      RESIS/RHOC    REACT/RHOC

    .000    1.84322E-05     .00    0.00000E+00     .00000       .00000
 125.000    4.96309E-05     .00    2.05345E-02    -.00006      -.00001
 250.000    4.15485E-05     .00    5.70915E-02     .00000       .00002
 375.000    4.35998E-05     .00    1.36698E-01     .00001       .00000
 500.000    5.61563E-05     .00    3.11184E-01     .00000       .00000
 625.000    7.44867E-05     .00    6.98051E-01     .00000       .00000
 750.000    1.32280E-04     .00    1.51042E+00     .00000       .00000
 875.000    6.32457E+02  130.00    8.00341E+00     .77985     -1.73821
1000.000    6.32457E+02  130.00    9.62628E+00     .85589     -1.33280
1125.000    6.32458E+02  130.00    1.13897E+01     .88111     -1.00787
1250.000    6.32458E+02  130.00    1.32377E+01     .88617      -.73581
1375.000    6.32457E+02  130.00    1.53689E+01     .85339      -.50597
1500.000    6.32457E+02  130.00    1.82088E+01     .78394      -.29433
1625.000    6.32457E+02  130.00    2.36269E+01     .64530      -.00767
1750.000    6.32458E+02  130.00    2.07269E+01     .67415       .29444
1875.000    6.32458E+02  130.00    1.89357E+01     .64474       .48240
2000.000    6.32458E+02  130.00    1.75159E+01     .54415       .67946
2125.000    2.93880E-04    3.34    7.70186E+00     .00000       .00000
```

The results of the computation are found in the last table.  A plot of the calculated impedance is shown in Figure 6.

28
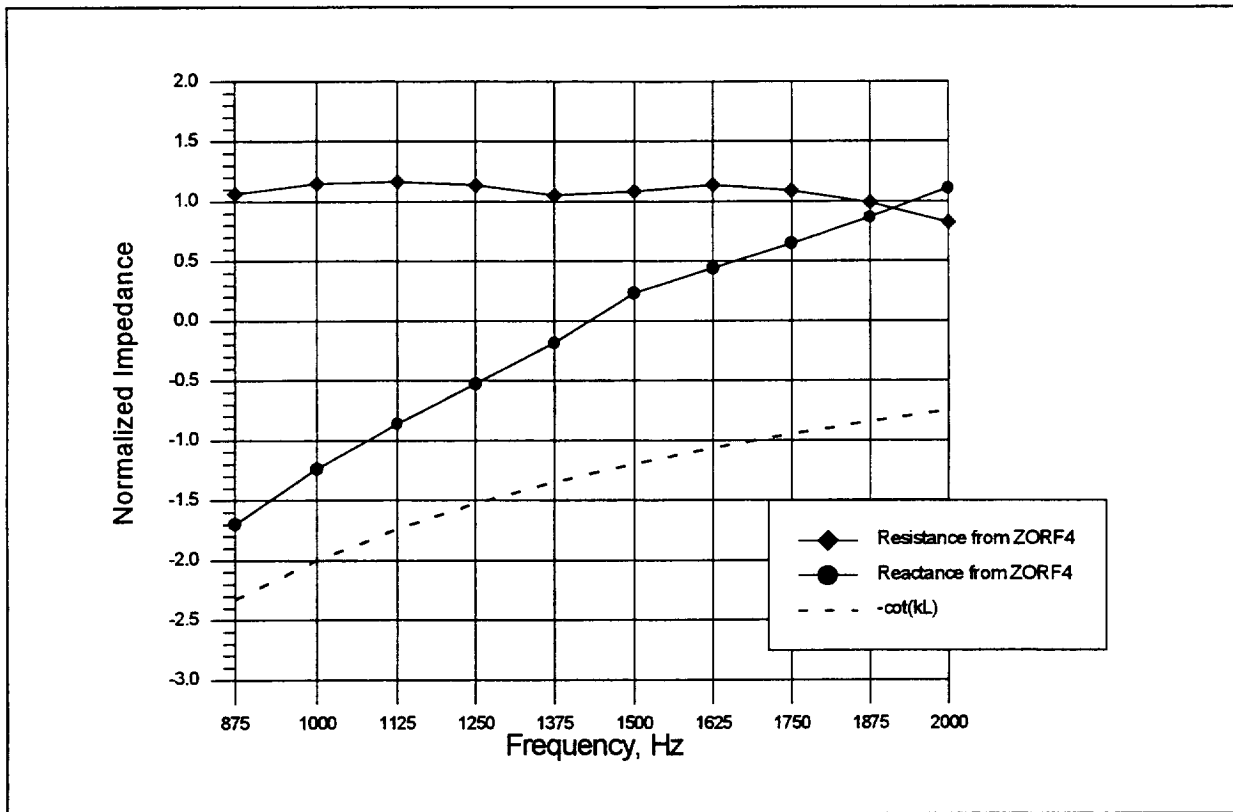
**Figure 6.**    **Computation of impedance by ZORF4 for sample case.**

The convergence of the numerical integration solution depends critically upon the number of grid points per wavelength used for the computation. Table 1 below shows the solution convergence comparing calculations with 100 and 200 points per wavelength. Notice that the solution has converged out to the third decimal place.

| | 100 pts/wavelength | | 200 pts/wavelength | |
|---|---|---|---|---|
| **Frequency** | **Resistance** | **Reactance** | **Resistance** | **Reactance** |
| 875 | 0.7811 | -1.72875 | 0.77985 | -1.73821 |
| 1000 | 0.85565 | -1.32442 | 0.85589 | -1.3328 |
| 1125 | 0.88038 | -0.9995 | 0.88111 | -1.00787 |
| 1250 | 0.88628 | -0.72759 | 0.88617 | -0.73581 |
| 1375 | 0.85283 | -0.49994 | 0.85339 | -0.50597 |
| 1500 | 0.77984 | -0.28886 | 0.78394 | -0.29433 |
| 1625 | 0.64522 | 0.00498 | 0.6453 | -0.00767 |
| 1750 | 0.6785 | 0.30041 | 0.67415 | 0.29444 |
| 1875 | 0.64803 | 0.48742 | 0.64474 | 0.4824 |
| 2000 | 0.54877 | 0.68181 | 0.54415 | 0.67946 |

**Table 1.**    **Comparison of ZORF4 impedance computation convergence for 100 and 200 points per wavelength.**

29

ZORF4 also creates four auxiliary data files. The most useful file is the ASCII table of pressure, velocity, and impedance versus frequency, for it can be imported easily into a plotting program. Users should be aware that the transient time history data files can become several megabytes large. Unless the transient behavior is of interest, these files should be deleted.

## 4.7. Check for Transient Decay

Assurance is needed that transients in the solution caused by "switching on" the pressure excitation at time zero have decayed to the point of having negligible effect on the impedance determination. It is assumed that the natural damping in the facesheet will act to attenuate these transients in the numerical integration.

The time constant used to attempt to achieve transient elimination is the period of the lowest frequency component in the pressure excitation (assuming no zero-frequency component). The pressure excitation "ramps up" linearly over the first three (or more) longest periods plus four cavity traverse times as the default settling time condition.

The user has an option of adding an arbitrary number of additional long period cycles to the settling time. The sample case defined in Section 4.6 was run with two different transient settling times, first with no extra periods in the settling time (default condition), and then with an additional five longest periods added, and the results were compared.

Table 2 shows the comparison of the impedance calculation at each frequency for the two different transient decay times. The excellent agreement can be noted, indicating acceptable convergence for this case. The actual time history of the acoustic particle displacement transient for the default settling time case, up to the time of initiation of data acquisition, is shown in Figure 7.

| Frequency, Hz. | Normalized Impedance | | | |
| --- | --- | --- | --- | --- |
| | Decay time = 0.00372 sec | | Decay time = 0.00944 | |
| 875 | 1.0593 | -1.7051i | 1.0629 | -1.7007i |
| 1000 | 1.1487 | -1.2332i | 1.1491 | -1.2396i |
| 1125 | 1.1681 | -0.8660i | 1.1652 | -0.8613i |
| 1250 | 1.1296 | -0.5240i | 1.1365 | -0.5275i |
| 1375 | 1.0632 | -0.1864i | 1.0511 | -0.1842i |
| 1500 | 1.0705 | 0.2379i | 1.0862 | 0.2333i |
| 1625 | 1.1525 | 0.4354i | 1.1416 | 0.4420i |
| 1750 | 1.0864 | 0.6511i | 1.0930 | 0.6485i |
| 1875 | 0.9971 | 0.8686i | 0.9916 | 0.8667i |
| 2000 | 0.8238 | 1.1052i | 0.8258 | 1.1094i |

**Table 2    Comparison of impedance computation for two transient decay times.**
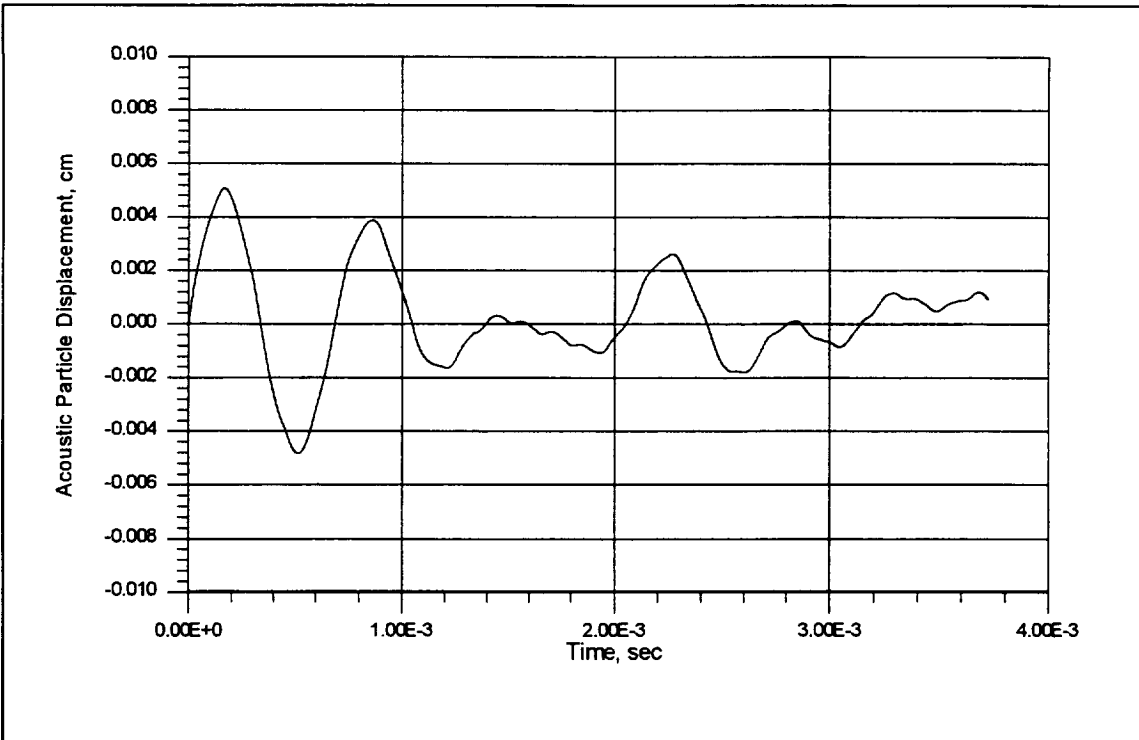
**Figure 7.** **Transient of acoustic particle displacement for sample case, default settling time.**

Since the Fourier transforms and averaging were taken for two different samples, some of the difference may be due to differences in the time samples, as opposed to being caused by the transient. In any case, neither cause has led to large differences. Further parametric studies are required before concluding unequivocally that there is no transient decay problem or to develop generalized acceptable decay time rules.

31

# 5. Comparison of Time-Domain Prediction to Frequency-Domain Models

## 5.1. Relation of Parameters to Current Impedance Models

The quantities m, $R_L$, and $R_{NL}$ are related to the physical parameters in the perforated facesheet. Conventionally-used models are discussed in detail in Reference[16]. In this section, we will first consider the mass reactance and then the resistance.

The mass reactance of a perforated sheet is given by

$$\frac{X_m}{\rho c} = \frac{2\pi f(t + \varepsilon d)}{c\sigma C_d} \tag{72}$$

where t is the facesheet thickness, d is the hole diameter, and $\varepsilon$ is an end correction coefficient. The effective orifice length is given by

$$\ell = t + \varepsilon d \tag{73}$$

Various expressions for the end correction coefficient $\varepsilon$ are discussed in Reference 16.

From Equation (28), we can identify m as a factor in the mass reactance, such that

$$X_m = -\frac{2\pi f}{c} m = -km = k\frac{\ell}{\sigma C_d} \tag{74}$$

It is important to note that the expression for mass reactance in Equation (74) differs from that in Reference 16 by the presence of the orifice discharge coefficient in the denominator. Most derivations of mass reactance for a perforate omit this factor. Since the effective orifice length is usually empirically-determined, any effect of the $1/C_d$ factor is incorporated into the effective orifice length.

The mass reactance is known to vary with the acoustic velocity amplitude (that is, with SPL) as well as being proportional to frequency. The variation with porosity may be more complex than a simple inverse variation. In order to be able to model the effects on mass reactance of the velocity-dependence of the slug of air in the orifice (the effective length) and the possibly independent variation of the orifice discharge coefficient separately, the form that has $C_d$ in the denominator is chosen here.

A commonly used expression for the linear part of the DC flow resistance is

$$R_L = \frac{32\rho\upsilon t}{\sigma C_d d^2} \tag{75}$$

where $\nu$ is the kinematic viscosity. A model for the coefficient of the nonlinear part of the DC flow resistance is

$$R_{NL} = \frac{\rho}{2(\sigma C_D)^2}$$  (76)

Some interpretations are necessary to adapt these models for use in ZORF4. The empirical rule for the equivalence of DC flow resistance measurements and acoustic faceplate resistance is to identify the DC flow incident velocity with the rms acoustic incident velocity.

From Equation (1), the DC flow resistance across the facesheet is given by

$$R_{DC} = \frac{\Delta p_{DC}}{U} = A + BU$$  (77)

where U is the incident DC flow velocity incident upon the facesheet. The coefficients A and B are the measured linear and nonlinear DC flow resistance coefficients, respectively. The corresponding acoustic resistance is given by

$$R_{AC} = R_{LIN} + R_{NL} u_{rms}$$  (78)

where $u_{rms}$ is the rms acoustic particle velocity. Assuming the equivalence of the resistance for the DC flow and the acoustic cases, and the equivalence of U and $u_{rms}$ , we identify $R_{LIN} = A$ and $R_{NL} = B$.

The frequency-domain impedance models use the assumption that $u_{rms}$ can be identified with the DC flow velocity to determine the faceplate resistance at any given frequency. Due to what is called a "bias effect", it has been found that the validity of the frequency-domain models can be improved by making the additional assumption that $u_{rms}$ is the overall rms acoustic velocity, integrated over the entire frequency spectrum. This leads to a predicted resistance that is essentially constant with frequency, since the overall $u_{rms}$ is the same at each frequency.

The assumption for the time-domain model is that the instantaneous flow resistance across the facesheet is given by the DC flow resistance relationship where U is identified with the instantaneous value of velocity as computed by the numerical integration. In this manner, the faceplate velocity contains all frequency components. This may reproduce the frequency-domain bias effect, but should maintain any effects of variation in pressure frequency spectrum shape. The issue is whether the DC flow measurement coefficients A and B are appropriate for the time-varying acoustic flow, or whether more sophisticated models are required. This issue must ultimately be resolved by comparison with experimental data.

The objectives for developing the time-domain model are to confirm or improve the perforated faceplate resistance and mass reactance models based on insight gained from the results of the numerical computations and their comparison to measured data. The numerical

model allows fine-tuning of the effects of variation of any of the parameters that make up the impedance model, such as the orifice discharge coefficient or effective orifice length.

## 5.2. Comparison of Time-Domain and Frequency-Domain Predictions

### 5.2.1. Multiple-Frequency Nonlinear Sample Case

The impedance of the treatment panel defined in the sample case in the previous section was predicted using a current frequency-domain model. Figure 8 shows a comparison of the impedance predicted by the time-domain model and the frequency-domain model.
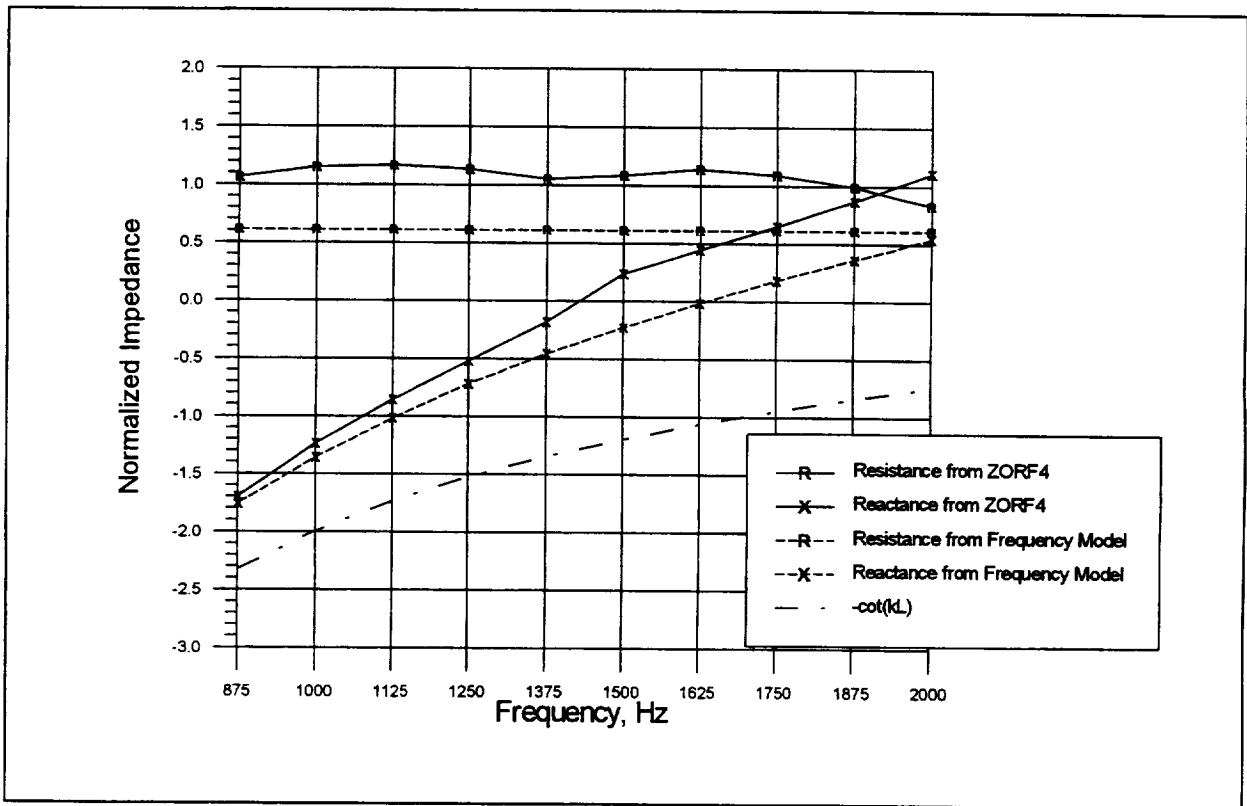


**Figure 8.** Comparison of time-domain and frequency-domain predicted impedances.

Note that, for this particular case, the time-domain model predicts both higher resistance and reactance. The added reactance is caused primarily by a higher prediction of mass reactance by the time-domain model. This reflects the use of the $C_d$ factor in the denominator of the time-domain model and its absence in the frequency-domain model. Note that the resistance predicted by the time-domain model is relatively flat, but not perfectly flat like the prediction for the frequency-domain model.

As we shall see later, one cannot at this point make the generalization that the time-domain model always over-predicts the resistance or mass reactance. Each case must be

34

examined individually. The ultimate resolution of model accuracy must come from comparison with experimentally-measured values, and this will be the subject of the following section.

### 5.2.2. Linearized Multiple-Frequency Sample Case

In the previous section, we found a disagreement between the time-domain and frequency-domain impedance models both with regard to nonlinear resistance and mass reactance. Assurance is needed that the two models give equivalent results for a case where the discrepancies caused by the nonlinear resistance iteration and the assumptions about the presence of the discharge coefficient in the mass reactance denominator are eliminated.

In this section, a sample case is considered in which the resistance is purely linear and the discharge coefficient is included in the mass reactance term for both models. The faceplate parameters remain the same as the previous sample case.

To linearize the resistance in the frequency-domain model, the DC flow resistance B-coefficient is set arbitrarily to zero and a grazing flow effect for Mach 0.1 is added to give a total resistance of 1.017 $\rho c$. In the time domain model, then, the $R_{LIN}$ input is set equal to 1.017 $\rho c$ and the $R_{NL}$ input is set equal to zero. The results of the predictions are shown in Table 3.

| Frequency | Frequency Domain | | Time Domain | |
|---|---|---|---|---|
| | Resistance | Reactance | Resistance | Reactance |
| 875 | 1.0169 | -1.5859 | 1.0199 | -1.5782 |
| 1000 | 1.0169 | -1.1522 | 1.0202 | -1.1455 |
| 1125 | 1.0169 | -0.7866 | 1.0199 | -0.7805 |
| 1250 | 1.0169 | -0.4688 | 1.0202 | -0.4631 |
| 1375 | 1.0169 | -0.1854 | 1.0199 | -0.1802 |
| 1500 | 1.0169 | 0.0721 | 1.0201 | 0.0773 |
| 1625 | 1.0169 | 0.3099 | 1.0200 | 0.3145 |
| 1750 | 1.0169 | 0.5324 | 1.0199 | 0.5372 |
| 1875 | 1.0169 | 0.7426 | 1.0201 | 0.7469 |
| 2000 | 1.0169 | 0.9431 | 1.0198 | 0.9477 |

**Table 3.** **Comparison of linear impedance predicted by frequency-domain and time-domain methods.**

Note the excellent agreement, assuring that there are no fundamental differences between the frequency-domain computation and the time-domain computation, at least for this linear sample case.

## 6. Comparison of Predicted and Measured Impedance

### 6.1. Single-Frequency Pressure Excitation

Normal incidence impedance tube measurement data were obtained for two perforated plate facesheets using pure tone excitation of a known SPL. The two perforates differ primarily in their porosity, and are defined in Table 4.

| Parameter | Faceplate 1 | Faceplate 2 |
|---|---|---|
| Porosity | 0.045 | 0.157 |
| Thickness, inches | 0.032 | 0.032 |
| Hole diameter, inches | 0.060 | 0.050 |
| Cavity depth, inches | 0.75 | 0.75 |
| Frequency, Hz. | 1500 | 3000 |
| Linear Resistance, cgs Rayls | 0.594 | 0.245 |
| Nonlinear Resistance, cgs Rayls/cm | 0.526 | 0.0432 |
| Effective Orifice Length, cm | 0.192 | 0.159 |

**Table 4.** Facesheet definition for single frequency predicted and measured impedance comparison.

Two SPL values are used in each case, 130 dB and 140 dB. Tables 5 and 6 are comparisons of impedances predicted using the frequency-domain model both with and without the $C_d$ factor in the denominator of the mass reactance, the time-domain model, and the measured value.

| Plate 1 - 4.5% Porosity | Normalized Impedance | |
|---|---|---|
| Model | 130 dB | 140 dB |
| Measurement | 0.587 - 0.222i | 1.874 - 0.489i |
| Time-domain model with $C_d$ in mass reactance | 0.464 - 0.177i | 0.839 - 0.165i |
| Frequency-domain with $C_d$ in mass reactance | 0.416 - 0.201i | 0.761 - 0.201i |
| Frequency-domain no $C_d$ in mass reactance | 0.303 - 0.570i | 0.678 - 0.570i |

**Table 5.** Comparison of predicted and measured impedance for Faceplate #1.

| Plate 2 - 15.7% Porosity | Normalized Impedance | |
|---|---|---|
| Model | 130 dB | 140 dB |
| Measurement | 0.188 + 0.1248i | 0.330 + 0.069i |
| Time-domain model with $C_d$ in mass reactance | 0.104 + 0.155i | 0.221 + 0.155i |
| Frequency-domain with $C_d$ in mass reactance | 0.092 + 0.151i | 0.199 + 0.151i |
| Frequency-domain no $C_d$ in mass reactance | 0.123 - 0.024i | 0.222 - 0.024i |

**Table 6.** Comparison of predicted and measured impedance for Faceplate #2.

The comparisons show mixed results. Generally, all models tend to under-predict the measured resistance. For both cases, the reactance values tend to bracket the measured value. No clear advantage can be seen for either the time-domain or the frequency-domain models, but it is also obvious that the time-domain model is not generating large errors. One can conclude that both models require improvement in the modeling of the resistance and mass reactance of the perforate if increased accuracy is the objective.

## 6.2.    Multiple-Frequency Pressure Excitation

An acoustic impedance measurement was performed by Rohr, Inc using a perforate plate SDOF treatment with the following parameters:

Porosity = 4.43%
Hole diameter = 0.0453 inches = 0.1151 cm.
Faceplate thickness = 0.031 inches = .07874 cm.
Cavity depth = 0.75 inches = 1.905 cm.

The measurement temperature was 67.9 degF. The treatment was excited by a fairly flat broadband pressure spectrum with an overall SPL of 149 dB. The time-domain prediction was made by combining the original measured 8 Hz. binwidth measured spectral pressure values into far fewer 576 Hz. bins. This was required by numerical computation problems encountered in the ZORF4 runs.

Figure 9 is a comparison of the measured impedance with the predictions from the frequency-domain and the time-domain models. The following observations can be made:

- The frequency-domain model predicts the measured resistance quite closely. The measured impedance is quite flat, although some variation not predicted by the frequency-domain model can be observed.
- The frequency-domain model overpredicts the mass reactance by a significant amount. This is in part due to the inclusion of the $1/C_d$ term in the mass reactance for this prediction. This factor was included to be able to compare the results directly to the time-domain prediction.
- The time-domain model overpredicts the measured resistance by a large amount above about 1700 Hz.
- The time-domain model shows a large overprediction of the mass reactance.
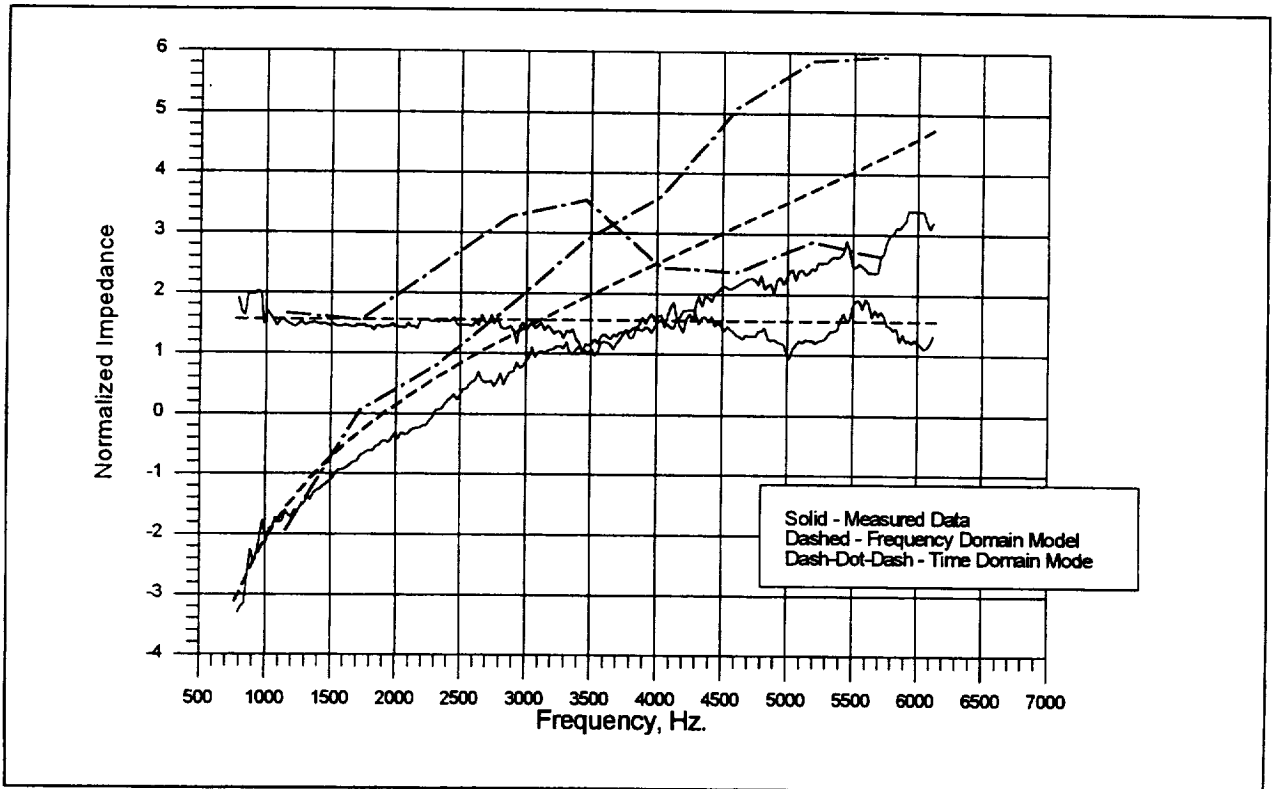
**Figure 9.** **Comparison of measured and predicted frequencies for SDOF treatment with broadband pressure excitation.**

The extreme overprediction of resistance and mass reactance by the time-domain model appears to be characteristic of the computation for high SPL values and multiple frequency input. The problem is exacerbated by large numbers of pressure frequencies, under which condition the computation will go unstable. The problem is caused by a combination of the nonlinear resistance algorithm, the high SPL levels, and the large number of pressure frequencies, because it is not experienced for the same case but with a linearized resistance. Further work is needed to examine the behavior of the nonlinear resistance algorithm.

# 7. Recommendations for Further Research

A more efficient finite difference integration algorithm is needed both to improve accuracy and reduce computation time. The objective of the development of this program, to obtain an operational computation under the simplest of analytical conditions, has been met, but this upgrade is needed to improve the utility of the program. Numerous improved algorithms are available, and one that should receive strong consideration is the dispersion-relation-preserving finite difference scheme of Tam[17,18].

The validity of the algorithm for the nonlinear impedance effects needs to be checked further, particularly for multiple-frequency cases. Possibly an improved finite difference algorithm may improve the nonlinear iteration, as well. This effort is necessary before the program can be used to examine effects of pressure frequency spectra shape.

Rather than expand the pressure Fourier series at each numerical integration time point, it may be possible to use Inverse Fast Fourier Transform techniques to generate the pressure time history for a complete data acquisition block. If this is possible with sufficient accuracy, this would speed the computation significantly.

The development and incorporation of more advanced resistance and mass reactance models for incorporation into the model is needed. In particular, the Reynold's number dependence of the orifice discharge coefficient and the velocity dependence (nonlinearity) of the mass reactance could be incorporated.

## 8. Nomenclature

| | |
|---|---|
| A | linear DC flow resistance coefficient |
| B | nonlinear DC flow resistance coefficient |
| c | speed of sound |
| $C_d$ | orifice discharge coefficient |
| $C_1 - C_6$ | numerical integration difference equation coefficients |
| d | perforate hole diameter |
| D | effective acoustic damping per unit area of faceplate |
| $D_1 - D_5$ | numerical integration difference equation coefficients |
| $F_{ph}$ | highest frequency present in pressure excitation spectrum |
| h | numerical integration time step |
| i | square root of $-1$ or integer index |
| j | integer index |
| k | wave number |
| $\ell$ | effective orifice length |
| L | cavity depth |
| m | mass reactance coefficient |
| M | effective acoustic mass per unit area of faceplate |
| N | number of spatial grid points in cavity |
| $N_{blk}$ | block size for data acquisition |
| NFP | number of non-zero pressure frequencies |
| $N_{frq}$ | number of frequency bins in frequency spectrum |
| $N_{ppl}$ | number of points per shortest wavelength in x-grid |
| $N_{samp}$ | number of numerical integration time intervals between each data sample |
| p | acoustic pressure |
| $PF_n$ | spectral component of applied pressure at $n^{th}$ frequency |
| $P_{fwd}$ | forward-traveling incident pressure wave amplitude |
| $p_{fwd}$ | forward-traveling part of incident pressure wave |
| R | resistance coefficient |
| $R_L$ | linear part of facesheet damping |
| $R_{NL}$ | nonlinear part of facesheet damping |
| SPL | Sound Pressure Level, dB, re: 0.0002 dynes/cm$^2$ |
| t | Facesheet thickness, also time |
| $T_1$ | interim variable for nonlinear numerical integration iteration |
| $T_{rec}$ | data block record time length |
| U | incident flow velocity for DC flow resistance measurement |
| $u_{rms}$ | rms value of acoustic velocity |
| v | acoustic particle velocity |
| $v_i$ | acoustic velocity in the $i^{th}$ frequency band |
| $V_n$ | $n^{th}$ spectral component of acoustic velocity |
| x | spatial variable along cavity |
| $X_n$ | $n^{th}$ spectral component of acoustic displacement |
| $Z_n$ | $n^{th}$ spectral component of acoustic impedance |

| | |
|---|---|
| $\alpha$ | normalized acoustic admittance |
| $\varepsilon$ | mass reactance end correction coefficient |
| $\Delta f$ | Fourier analysis frequency resolution, bin size |
| $\Delta t$ | grid time step size |
| $\Delta x$ | grid spatial step size |
| $\lambda$ | wavelength |
| $\mu$ | absolute viscosity |
| $\nu$ | kinematic viscosity, $\mu/\rho$ |
| $\rho$ | medium density |
| $\sigma$ | perforate open area ratio, or porosity |
| $\tau$ | numerical integration time step parameter, $= ct$ |
| $\omega$ | circular frequency |
| $\xi$ | acoustic particle displacement |
| $\xi_M$ | interim variable for nonlinear numerical integration iteration |
| $\xi_P$ | interim variable for nonlinear numerical integration iteration |

# 9. References

[1] Motsinger, R. E., and Kraft, R. E., "Design and Performance of Duct Acoustic Treatment", Chapter 14 in Hubbard, Harvey H., ed., *Aeroacoustics of Flight Vehicles: Theory and Practice, Volume 2: Noise Control*, NASA Reference Publication 1258, Vol. 2, 1991.

[2] Rice, Edward J., "A Model for the Acoustic Impedance of a Perforated Plate Liner with Multiple Frequency Excitation", NASA TM X-67950, October, 1971.

[3] Cummings, A., "Transient and Multiple Frequency Sound Transmission Through Perforated Plates at High Amplitude", AIAA 84-2311, October, 1984.

[4] Zorumski, William E. and Parrott, Tony L., "Nonlinear Acoustic Theory for Thin Porous Sheets",NASA SP-189, October, 1968.

[5] Zorumski, William E. and Tester, Brian J., "Prediction of the Acoustic Impedance of Duct Liners", NASA TM X-73951, September, 1976.

[6] Rice, Edward J., "A Model for the Pressure Excitation Spectrum and Acoustic Impedance of Sound Absorbers in the Presence of Grazing Flow", AIAA 73-995, October, 1973.

[7] Hersh, A. S. and Rogers, T., "Fluid Mechanical Model of the Acoustic Impedance of Small Orifices", AIAA 75-496, March, 1975.

[8] Hersh, Alan. S. and Walker, Bruce, "Fluid Mechanical Model of the Helmholtz Resonator", NASA CR-2904, September, 1977.

[9] Hersh, A. S., "Nonlinear Behavior of Helmholtz Resonators", AIAA 90-4020, October, 1990.

[10] Cummings, A. and Eversman, W. "High Amplitude Acoustic Transmission Through Duct Terminations: Theory", Journal of Sound and Vibration, 91, 1983, pp.503-518.

[11] Press, W. H., Teukolsky, S. A., Vetterling, W. T., and Flannery, B. P., *Numerical Recipes in FORTRAN: The Art of Scientific Computing*, Cambridge University Press, Second Edition, 1992, pp. 825-831.

[12] Berezin, I. S. and Zhidkov, N. P., *Computing Methods: Volume II*, Pergamon Press, 1965, pp. 470-486.

[13] Smith, G. D., *Numerical Solution of Partial Differential Equations*, Oxford University Press, 1965, pp. 111-114.

[14] Fox, L., *Numerical Solution of Ordinary and Partial Differential Equations*, Pergamon Press, 1962, pp. 218-222.

[15] Lynn, P. A. and Fuerst, W., *Digital Signal Processing with Computer Applications*, John Wiley and Sons, 1989, p. 251.

[16] Motsinger, R. E., and Kraft, R. E., "Design and Performance of Duct Acoustic Treatment", Chapter 14 in Hubbard, Harvey H., ed., *Aeroacoustics of Flight Vehicles: Theory and Practice, Volume 2: Noise Control*, NASA Reference Publication 1258, Vol. 2, 1991, pp.180-181.

[17] Tam, Christopher K. W., and Webb, J. C., "Dispersion-Relation-Preserving Finite Difference Schemes for Computational Acoustics", Journal of Computational Physics, 107, 1993, pp. 262-281.

[18] Tam, C. K. W., "Computational Aeroacoustics: Issues and Methods", AIAA 95-0677, January, 1995.

# REPORT DOCUMENTATION PAGE

Public reporting burden for this collection of information is estimated to average 1 hour per response, including the time for reviewing instructions, searching existing data sources, gathering and maintaining the data needed, and completing and reviewing the collection of information. Send comments regarding this burden estimate or any other aspect of this collection of information, including suggestions for reducing this burden, to Washington Headquarters Services, Directorate for Information Operations and Reports, 1215 Jefferson Davis Highway, Suite 1204, Arlington, VA 22202-4302, and to the Office of Management and Budget, Paperwork Reduction Project (0704-0188), Washington, DC 20503.

| 1. AGENCY USE ONLY (Leave blank) | 2. REPORT DATE | 3. REPORT TYPE AND DATES COVERED |
|---|---|---|
| | April 1999 | Contractor Report |

| 4. TITLE AND SUBTITLE | 5. FUNDING NUMBERS |
|---|---|
| Acoustic Treatment Design Scaling Methods Volume 4: Numerical Simulation of the Nonlinear Acoustic Impedance of a Perforated Plate Single-Degree- of-Freedom Resonator Using a Time-Domain Finite Difference Method | C-NAS3-26617 TA 25 |
| **6. AUTHOR(S)** R. E. Kraft | WU-538-03-12-02 |

| 7. PERFORMING ORGANIZATION NAME(S) AND ADDRESS(ES) | 8. PERFORMING ORGANIZATION REPORT NUMBER |
|---|---|
| General Electric Aircraft Engines (GEAE) P. O. Box 156301 Cincinnati, OH 45215-6301 | |

| 9. SPONSORING/MONITORING AGENCY NAME(S) AND ADDRESS(ES) | 10. SPONSORING/MONITORING AGENCY REPORT NUMBER |
|---|---|
| National Aeronautics and Space Administration Langley Research Center Hampton, VA 23681-2199 | NASA/CR-1999-209120/VOL4 |

**11. SUPPLEMENTARY NOTES**

Lewis Project Manager: Christopher E. Hughes
Langley Technical Monitors: Tony L. Parrott, Lorenzo R. Clark
Prepared for Langley Research Center under Contract NAS3-26617, Task 25.

| 12a. DISTRIBUTION/AVAILABILITY STATEMENT | 12b. DISTRIBUTION CODE |
|---|---|
| Unclassified-Unlimited Subject Category 71 Distribution: Standard Availability: NASA CASI (301) 621-0390 | |

**13. ABSTRACT (Maximum 200 words)**

Single-degree-of-freedom resonators consisting of honeycomb cells covered by perforated facesheets are widely used as acoustic noise suppression liners in aircraft engine ducts. The acoustic resistance and mass reactance of such liners are known to vary with the intensity of the sound incident upon the panel. Since the pressure drop across a perforated liner facesheet increases quadratically with the flow velocity through the facesheet, this is known as the nonlinear resistance effect. In the past, two different empirical frequency domain models have been used to predict the Sound Pressure Level effect of the incident wave on the perforated liner impedance, one that uses the incident particle velocity in isolated narrowbands, and one that models the particle velocity as the overall velocity. In the absence of grazing flow, neither frequency domain model is entirely accurate in predicting the nonlinear effect that is measured for typical perforated sheets. The time domain model is developed in an attempt to understand and improve the model for the effect of spectral shape and amplitude of multi-frequency incident sound pressure on the liner impedance. A computer code for the time-domain finite difference model is developed and predictions using the models are compared to current frequency-domain models.

| 14. SUBJECT TERMS | | 15. NUMBER OF PAGES |
|---|---|---|
| Aircraft noise; acoustic treatment; fan noise suppression; scale models; acoustic impedance | | 50 |
| | | **16. PRICE CODE** A03 |

| 17. SECURITY CLASSIFICATION OF REPORT | 18. SECURITY CLASSIFICATION OF THIS PAGE | 19. SECURITY CLASSIFICATION OF ABSTRACT | 20. LIMITATION OF ABSTRACT |
|---|---|---|---|
| Unclassified | Unclassified | Unclassified | UL |